Dehydration of the Uranyl Peroxide Studtite, $[UO_2(\eta^2\text{-}O_2)(H_2O)_2]\cdot 2H_2O$, Affords a Drastic Change in the Electronic Structure: A Combined X-ray Spectroscopic and Theoretical Analysis

Tonya Vitova,*[,†] Ivan Pidchenko,[†] Saptarshi Biswas,[‡,#] George Beridze,[§,∥] Peter W. Dunne,[‡] Dieter Schild,[†] Zheming Wang,[⊥] Piotr M. Kowalski,*[,§,∥] and Robert J. Baker*[,‡]

[†]Institute for Nuclear Waste Disposal (INE), Hermann von Helmholtz Platz 1, D 76344 Eggenstein Leopoldshafen, Germany

[‡]School of Chemistry, University of Dublin, Trinity College, College Green, Dublin 2, Ireland

[§]Institute of Energy and Climate Research, IEK 6, Nuclear Waste Management and Reactor Safety, Forschungszentrum Jülich GmbH, Wilhelm Johnen Strasse, 52428 Jülich, Germany

[∥]JARA High Performance Computing, Schinkelstrasse 2, 52062 Aachen, Germany

[⊥]Pacific Northwest National Laboratory, MSIN K8 96, P.O. Box 999, Richland, Washington 99352, United States

ABSTRACT: The minerals studtite, $[UO_2(\eta^2\ O_2)(H_2O)_2]\cdot 2H_2O$, and metastudtite, $[UO_2(\eta^2\ O_2)(H_2O)_2]$, are uranyl peroxide minerals that are major oxidative alteration phases of UO_2 under conditions of geological storage. The dehydration of studtite has been studied using X ray photoelectron spectroscopy (XPS) and X ray absorption spectroscopy. XPS of the U 4f region shows small but significant differences between studtite and metastudtite, with the 4f binding energy of studtite being the highest reported for a uranyl mineral studied by this technique. Further information about the changes in the electronic structure was elucidated using U M_4 edge high energy resolution X ray absorption near edge structure (HR XANES) spectroscopy, which directly probes f orbital states. The transition from the 3d to 5fσ* orbital is sensitive to variations in the U═O_{axial} bond length and to changes in the bond covalency. We report evidence that the covalence in the uranyl fragment decreases upon dehydration. Photoluminescence spectroscopy at near liquid helium temperatures reveals significant spectral differences between the two materials, correlating with the X ray spectroscopy results. A theoretical investigation has been conducted on the structures of both studtite and metastudtite and benchmarked to the HR XANES spectra. These illustrate the sensitivity of the 3d to 5f σ* transition toward U═O_{axial} bond variation. Small structural changes upon dehydration have been shown to have an important electronic effect on the uranyl fragment.

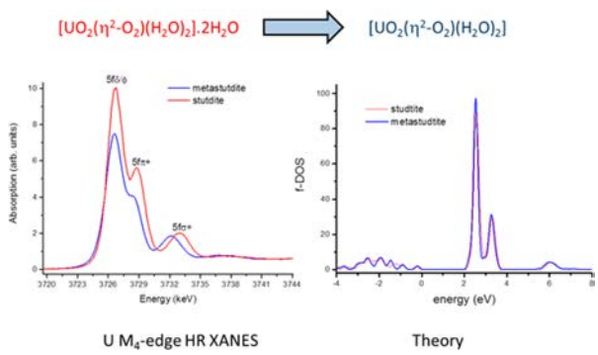

INTRODUCTION

The renaissance in actinide coordination chemistry over the past decade has, in part, been driven by the requirements to fully understand the chemistry that underpins separation science with respect to nuclear fuel reprocessing and the long term storage of nuclear waste in geological disposal facilities. The radiation load from a nuclear repository will generate H_2O_2 by α radiolysis of water, which can generate a local oxidizing environment under conditions that may be globally reducing. From studies targeting the potential speciation and reaction chemistry of UO_2 over long periods of time ($\sim 10^7$ years), one class of compounds that have generated much interest consists of the uranyl peroxides studtite, $[UO_2(\eta^2\ O_2)(H_2O)_2]\cdot 2H_2O$, and its dehydrated product metastudtite $[UO_2(\eta^2\ O_2)(H_2O)_2]$, and these are becoming more important in the underlying chemistry of a geological repository. Studtite and metastudtite can be formed by dissolution of UO_2 in the presence of H_2O_2,[1] or upon α,[2] β,[3] and γ[4] irradiation of UO_2 surfaces in contact with water. They have also been characterized on the surface of spent nucler fuel[5] and depleted uranium munitions discharged during the war in the Balkans.[6] Studtite has also been noted to act as a passivating layer for further dissolution when electroplated onto stainless steel, although this is dependent on the concentration of H_2O_2.[7] The pH is also important, as under alkaline conditions compounds such as $[UO_2(O_2)(CO_3)_2]^{4-}$,[8] $[(UO_2)_x(O_2)_y(OH)_z]^{n-}$ [$x = 1$, $y = 1$, $z = 2$, $n = 2$; $x = 1$, $y = 2$, $z = 2$, $n = 4$ (ref 9); $x = 1$, $y = 1$, $z = 1$, $n = 1$; $x = 2$, $y = 1$, $z = 1$, $n = 1$ (ref 10); $x = 1$, $y = 3$, $z = 0$, $n = 4$ (ref 11)], and, most spectacularly, uranyl nanosized clusters[12] can be formed. The latter have been proposed as a uranium speciation product in

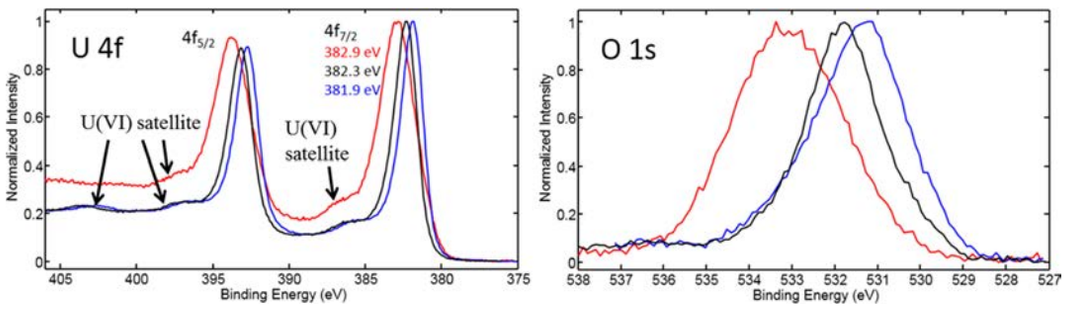

Figure 1. XPS narrow scans of U 4f and O 1s elemental lines of studtite (red), metastudtite (blue), and metaschoepite (black).

the reactors in the Fukushima Daiichi power plant.[13] The addition of ancillary ligands such as oxalates[14] or pyrophosphates[15] affords further building blocks for cluster assembly.

The thermodynamic stability of both studtite[16] and metastudtite[17] has been assessed using high temperature oxide calorimetry, and the dehydration of studtite to metastudtite has been found to be irreversible. Given that temperature will be a key factor in long term storage of spent nuclear fuels, the mechanism of dehydration is important to understand, and previous work using thermogravametric analysis[18] and variable temperature powder X ray diffraction has shown that studtite is stable to approximately 60−100 °C, at which point it forms metastudtite. This decomposes between 180 and 240 °C to form an amorphous phase of hydrated UO_3 followed by dehydration up to 500 °C and eventually U_3O_8. More recently on the basis of neutron scattering experiments[19] and thermochemical analysis,[20] this amorphous UO_3 was suggested to be U_2O_7, which contains a bridging peroxo and an oxo group; however, vibrational spectroscopic data suggest the presence of $[UO_{3-x}(OH)_{2x}]\cdot zH_2O$.[21] While the structure of naturally occurring studtite has been reported from single crystal X ray diffraction,[22] the only structural data for metastudtite have been acquired by using EXAFS at the U L_3 edge.[23] We also noted an unusual change in the electronic structure that could be difficult to rationalize on the basis of the removal of two interstitial water molecules in studtite that are not coordinated to the uranium center.[23] We wish to report further results obtained by spectroscopic and theoretical methods that probe this dehydration to metastudtite. In particular, a combination of X ray photoelectron spectroscopy (XPS), high energy resolution X ray absorption near edge structure (HR XANES) at the uranium M_4 absorption edge, to reduce the core−hole broadening, and emission spectroscopy at 8 K has corroborated our initial supposition that a significant electronic change occurs upon dehydration. Moreover, metastudtite appears to be electronically similar to metaschoepite, $[(UO_2)_4O(OH)_6]\cdot 5H_2O$. We have used theoretical methods to improve our understanding of the origin of this change.

RESULTS AND DISCUSSION

The samples of studtite, metastudtite,[23] and metaschoepite[24] used in our study were prepared following the procedure explained in our previous publication. We first examined the three compounds by XPS to ensure that the samples had the correct atomic concentrations (Table S1) and to ensure that no unexpected redox chemistry had occurred during the synthesis. XP survey spectra are shown in Figures S1 and S2 and narrow scans of U 4f and O 1s elemental lines in Figure 1.

Inspection of the U 4f region and the associated satellites confirms the absence of U(V) or U(IV), via synthesis or reduction by the X ray beam, but the binding energies of these peaks show differences. In the case of metastudtite, the spacings between the satellites and the main U 4f lines are 4.0 and 10.1 eV, characteristic of U(VI).[25] In the case of studtite, the spacings between the satellites and the main U 4f lines are 3.5 eV higher in binding energy than U 4f elemental lines and satellites at around 10 eV are not clearly detected. Interestingly, in comparison to other uranyl minerals studied by this technique, the U $4f_{7/2}$ peak for studtite [382.9 ± 0.2 eV; full width at half maximum (fwhm) = 2.8 eV] is the highest reported, but that of metastudtite (381.9 ± 0.2 eV; fwhm = 1.8 eV) is similar to that of metaschoepite (382.3 ± 0.2 eV; cf. 382.0 ± 0.1 eV in the literature[26]). These shifts are consistent with the shifts in the computed binding energies of the 6s states of U, the lowest energy states that have been computed explicitly. Taking the 6s binding energy in metastudtite as a reference, we obtained shifts of +1.4 and +0.2 eV for studtite and metaschoepite,[27] respectively; similar shifts of the different core electronic levels have been described.[28] The pronounced offset could indicate that the electronic density on U in studtite is lower than that in metastudtite and metaschoepite, which could lead to stronger attraction of the 4f and 6s electrons by the nucleus. However, our calculations of Bader charges show a nearly identical charge of U (within 0.01 e) in all three phases, which points toward a different origin of the shifts, such as, for instance, variation in the crystal field potential.[29] Similar shifts are observed in XPS spectra of O 1s states (Figure 1) but cannot be resolved into the individual components of U═O_{axial}, U−O_{peroxo}, and U−O_{water}, as has been noted for other uranyl minerals.[30]

The XPS data shed some light on the differences in electronic structure between studtite and metastudtite, but for more detailed information, we utilized HR XANES spectroscopy. We previously reported the U L_3 edge spectra of these compounds, and we were able to trace a change in the band gaps to the slight change in the U−O bond lengths upon dehydration.[23] The U L_3 edge HR XANES region of the spectra provided some evidence of this structural difference. However, given the limitations of measuring at this edge, particularly the large core−hole broadening contributing to the spectrum (≈4 eV),[31] we decided to look at the M_4 edge where this is reduced (≈0.3 eV);[32] notably, the number of HR XANES measurements at this edge is very limited. The studtite and metastudtite spectra are shown in Figure 2. The spectrum of metastudtite is slightly shifted to lower energies (≈0.1 ± 0.05 eV) compared to the spectrum of studtite (Figure S3), which is generally consistent with the offsets in binding energies observed in XPS spectra (*vide supra*). The fact that this energy

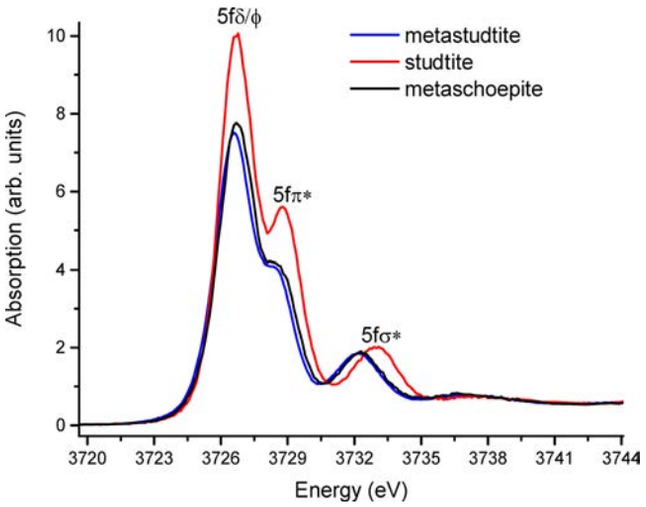

Figure 2. U M_4 edge HR XANES spectra of studtite (red), metastudtite (blue), and metaschoepite (black).

shift is very small substantiates the computational result that there are no significant variations in the electronic density on U.

The first three peaks of the uranyl M_4 edge HR XANES spectra have been assigned to transitions of 3d electrons to 5f δ/ϕ, π^*, and σ^* molecular orbitals with predominant 5f character.[33] Recently, it has been demonstrated for Pu(VI) plutonyl, which has a local coordination environment similar to that of uranyl, that the ligand field has a profound impact and is responsible for the appearance of more than one peak in the Pu M_5 edge HR XANES spectrum.[32c] Atomic multiplet calculations (using the DIRAC program system[34]) of Pu(VI) reproduce only the first main peak, whereas the spectrum computed with the finite difference method (FDMNES code)[35] taking into account the ligand field successfully calculates all spectral features. It was recently illustrated that the σ^* peak shifts toward the main 5f δ/ϕ peak when the overlap driven U═O_{axial} bond covalence decreases.[32c] This can potentially correlate with elongation of the U═O_{axial} bond.[36] The energy shift of the 5f σ^* peak compared to the 5f δ/ϕ peak is 6.2 ± 0.05 and 5.5 ± 0.05 eV for studtite and metastudtite, respectively (Figures S3 and S4). In addition, EXAFS at the U L_3 edge reported for metastudtite shows a very slight (+0.01 ± 0.01 Å) elongation of the U═O_{axial} bond and a more pronounced shortening of the equatorial U−O_{peroxo} bond (−0.04 ± 0.01 Å).[23] This experimental evidence suggests that the covalence of the U═O_{axial} bond has decreased for metastudtite compared to that of studtite upon dehydration. Currently, there are no experimental or theoretical indications in the literature that this energy shift between the 5f σ^* and 5f δ/ϕ peaks can be caused by other effects. Interestingly, after storage of a sample of studtite in air for 20 months, the energy positions of the spectral peaks are very similar to those of metastudtite, suggesting comparable electronic structure (Figure S5). We do not attempt here to interpret differences in intensities because they can be easily influenced by, for example, self absorption effects. From thermodynamic measurements,[16,17] dehydration is an irreversible process, and this observation gives further experimental proof.

Given that XPS and emission spectroscopy (*vide supra*) suggest that metaschoepite and metastudtite are similar, we have measured the uranium M_4 edge spectrum of metaschoepite, and this is shown in Figure 2. Importantly, the lengths of the U═O_{axial} (average of 1.759 Å), U−O (2.208 Å), and U−OH (2.41−2.58 Å) bonds determined from a crystallographic study[27] compare well to that of metastudtite, although metaschoepite has a pentagonal bypyramidal UO_7 geometry compared to the octahedral UO_6 geometry for metastudtite. In addition, the band gaps measured at the absorption edge in the diffuse reflectance ultraviolet−visible spectrum of 3.45, 2.71, and 2.66 eV for studtite, metastudtite,[37] and metaschoepite (Figure S6), respectively, suggest an electronic likeness between metastudtite and metaschoepite. Therefore, there is a local structural and electronic similarity between metastudtite and metaschoepite, which is reflected in the HR XANES spectra in both the M_4 and L_3 edge[23] spectra.

It is clear from the X ray spectroscopy that the uranyl unit is perturbed upon dehydration, and luminescence spectroscopy can be used to further probe this effect. We have reported that both studtite and metastudtite are non emissive at room temperature and when cooled to 77 K.[37] Recently, it has been demonstrated that cooling samples to liquid helium temperatures provides a dramatic enhancement of the emission intensity,[38] likely corresponding to the suppression of phonon assisted energy transfer. The cryogenic luminescence spectra of studtite and metastudtite displayed dramatic differences in their spectral profiles, spectral intensities, and luminescence decay behavior (Figures 3 and 4 and Figure S7). The studtite spectra

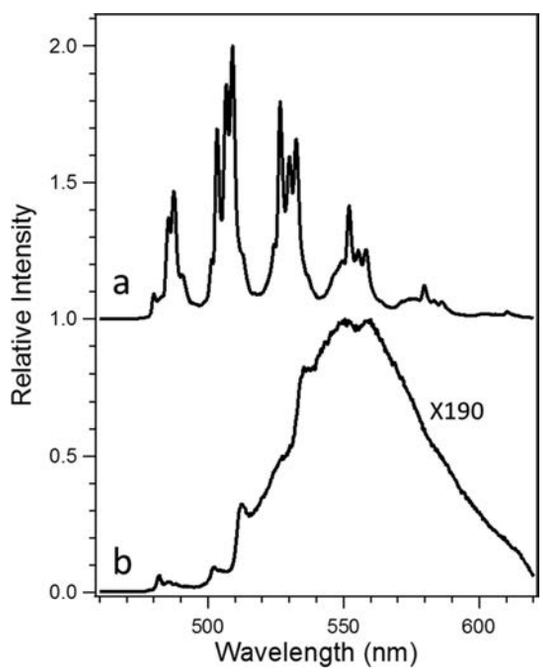

Figure 3. Laser induced luminescence emission spectra of (a) studtite and (b) metastudtite at near liquid helium temperature (T = 8 ± 2 K; λ_{em} = 415 nm). The spectra were normalized to unity intensity with the relative scaling factor labeled.

consist of a series of well resolved, even spaced vibronic bands. The average vibronic band spacing of 878 cm^{-1} is one of the largest observed among uranyl compounds,[38] indicating strong U═O_{axial} bonds; this can be compared to the vibrational band at 819 cm^{-1} as measured by Raman spectroscopy.[39] Time resolved luminescence spectra of studtite at delay times of >5 ms showed that the primary spectral features remained at all delay times (Figure 3), although the fine details among each of

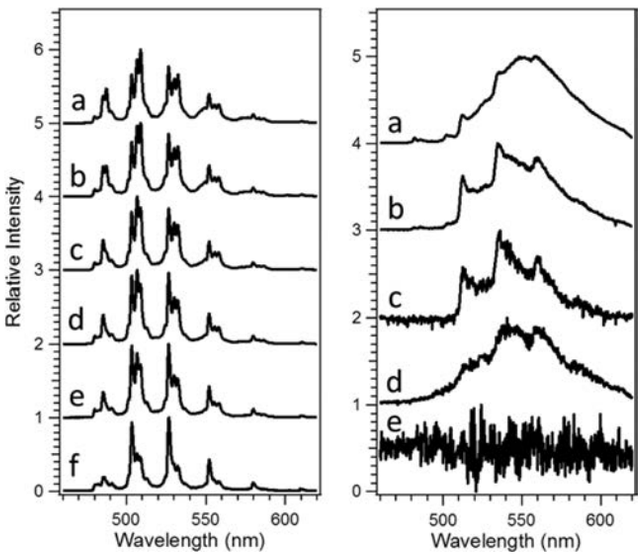

Figure 4. Laser induced time resolved luminescence emission spectra at different delay times of studtite (left) and metastudtite (right) at near liquid helium temperature (T = 8 ± 2 K; λ_{em} = 415 nm). The spectra were normalized to unity intensity and offset along the intensity axis for the sake of clarity. The delay time and time gate width are (a) ≤5 ns and 100 μs, (b) 100 and 100 μs, (c) 400 and 100 μs, (d) 900 and 200 μs, (e) 1500 and 200 μs, and (f) 4100 and 500 μs, respectively.

the vibronic bands evolve in a systematic way where the relative intensity of the peaks with lower energies (longer wavelength) decreased as the delay time increased. The exact mechanism of this spectral change is not clear. It could be due to time dependent relaxation of coupling between the electronic and vibrational transitions or the presence of more than one crystalline phase of the same studtite structure under cryogenic conditions.

In contrast, the spectra of metastudtite show a single broad band with the peak maximum red shifted ∼40 nm to 550 nm and a relative intensity of ∼0.5% as compared to those of studtite. Both the spectral profile and the spectral position are similar to those of metaschoepite[38] as well as uranium doped in borosilicate glasses,[40] indications of uranyl in a less crystalline and significantly distorted environment. The weak luminescence intensity clearly indicates that structural changes during the dehydration of studtite allow for more efficient deactivation pathways of the uranyl excited state. Time resolved spectra (Figure 3) showed that the primary features of the spectra gradually disappeared as the delay time increased, and at least two additional spectral profiles emerged at intermediate to long delay times (Figure 4b−d), suggesting the presence of more than one uranyl coordination environment or the generation of minor impurities during the mineral transformation process. Consistent with the spectral changes, the fitting of the luminescence decay of metastudtite (as well as studtite) required a minimum of two exponential functions, and the resulting luminescence lifetimes of metastudtite were significantly shorter than those of studtite: 862 μs (dominant) and 143 μs for studtite and 28 μs (dominant) and 123 μs for metastudtite (Figure S7).

While we routinely check the purity of our synthetic samples by powder X ray diffraction, we have additionally analyzed the data via a Rietveld refinement for metastudtite. The details are recorded in Figure S8 and Tables S3−S5, but the most pertinent factor is the bending of the O═U═O moiety [$\angle_{O-U-O}$ = 168.418(1)°]. Given the limitations of this method, and the paucity of bent uranyls in the literature,[41] we do not give significant weight to the analysis. A recent review of bending in uranyls suggests this could be due to electronic or, in this case unlikely, steric effects.[42] Nonetheless, it could explain the results of luminescence spectroscopy (if the uranyl bends, then the coupling of the symmetric U═O vibration will be partially lost and the well resolved bands no longer observable), and we note that further dehydration of metastudtite may form the U_2O_7 moiety with a bent uranyl.[19] It is possible that one of the structural consequences of dehydration of studtite is an increasing bending of the uranyl moiety, and further investigations will be published in due course.

Our spectroscopic investigations have indicated a change in the uranium electronic structure, so we next initiated a thorough computational investigation. The lattice parameters of the computed structures are listed in Table 1 and compared to the experimental single crystal X ray diffraction data for studtite[22] and previous theoretical studies. Although detailed structural information about metastudtite is not available, the lattice parameters of this mineral have been measured by powder diffraction patterns by us (Figure S8) and reported by others.[43,44] Some studies have been published in which metastudtite was modeled *ab initio*[45,46] and are somewhat inconsistent. As a starting point, we used the structure calculated by Weck et al.,[46] which predicts metastudtite to be in orthorhombic space group *Pnma* (Z = 4). Ostanin et al.[45] proposed D_{2h} symmetry for metastudtite but reported a volume 4.3% larger than the experimental values reported by Deliens et

Table 1. Comparison of the Computed and Measured Lattice Parameters of Studtite and Metastudtite

	studtite				metastudtite				
method	V	a	b	c	V	A	b	c	ref
PBE+U	697.8	14.15	6.84	8.58	510.9	6.82	8.80	8.51	this work
PBESol+U	650.8	13.71	6.71	8.46	483.9	6.72	8.57	8.41	this work
PW91	685.6	13.93	6.84	8.55	497.4	6.75	8.72	8.45	46
PBE					502.1	6.80	8.68	8.51	45
PBE	669.9	13.81	6.80	8.50					49
exp	665.6(3)	14.068(6)	6.721(3)	8.428(4)					22
						6.51(1)	8.78(2)	4.21(1)	43
					478.39	8.411(1)	8.744(1)	6.505(1)	44
						8.4184(4)	8.7671(4)	6.4943(3)	17
					480.88(7)	8.4164(7)	8.7787(7)	6.5085(5)	this work

Table 2. Computed and Experimental[23] U−O Bond Lengths (in angstroms) for Studtite and Metastudtite

	studtite			metastudtite		
bond	EXAFS	PBE+*U*	PBEsol+*U*	EXAFS	PBE+*U*	PBEsol+*U*
U O_{axial}	1.78	1.81	1.81	1.79	1.79	1.78
					1.82	1.83
U O_{peroxo}	2.36	2.42	2.40	2.32	2.43	2.40
		2.44	2.41			
U O_{water}	2.50	2.45	2.39	2.52	2.47	2.41

al.[43] and Rodriguez et al.[44] and 1% larger than the computed result of Weck et al.[46] It has to be noted that the mismatch in volumes also strongly depends on the density functional theory (DFT) functional and the computational methodology. The structural details of these calculations are provided for comparison in Table 1. In our calculations, the PBE+*U* method slightly overestimates the lattice parameters by ∼5% in terms of volume, which is a common feature of this particular functional.[47] This is illustrated by a better fit to the experimental lattice parameters when the PBEsol functional was used in the calculations. This is expected as the PBEsol functional is a modification of the PBE functional, which improves the prediction of structural parameters, however, often at the cost of making the description of other properties worse.[48] However, despite these differences, the lattice parameters of both phases are relatively well reproduced, with our PBEsol+*U* approach giving a match to the experimental volumes better than that of the previous computational studies.[45,46]

The structural parameters of the minerals computed with the DFT+*U* method are listed in Table 2. The computations result in nearly identical U═O_{axial} and U−O_{peroxo} bond lengths for the two phases, with slightly different U═O_{axial} bond lengths in each phase. As a result, the *f* density of states (*f* DOS), plotted in Figure 5 (solid line), is nearly identical, which does not reflect the differences seen in the experimental HR XANES spectra. We therefore modified our structures so that they

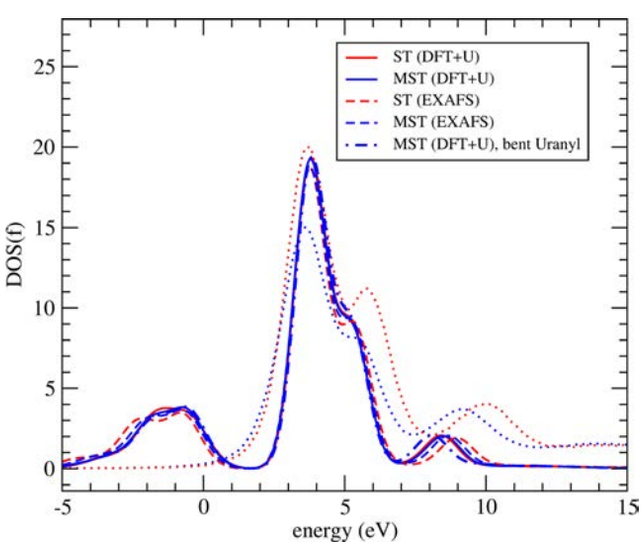

Figure 5. *f* DOS calculated with the DFT+*U* method for relaxed DFT +*U* structures and their modified versions reflecting EXAFS U−O bond lengths (dashed lines) and bending of uranyl (with an O═U═O angle of 168.5°), which are essentially indistinguishable from the unperturbed structure. The dotted lines represent the experimentally determined U M edge HR XANES. ST, studtite; MST, metastudtite.

reflect the EXAFS measurements of U−O bond lengths.[23] The *f* DOS values computed on these structures are given in Figure 5 (dashed line), and a closer match to the M_4 edge HR XANES is observed. The low intensity peak at 9 eV, corresponding to the 5f σ^* transition, is shifted to lower energies in the case of metastudtite, with the offset being consistent with the HR XANES measurements. The most intense peak at 4 eV, corresponding to the 5f δ/ϕ transition, is also qualitatively well reproduced. To further probe the origin of the relative differences between the HR XANES spectra of the two phases, we computed the DFT+*U* structures with U−O_{peroxo} bond lengths manually shifted by 0.05 Å. As shown in Figure 6, the *f*

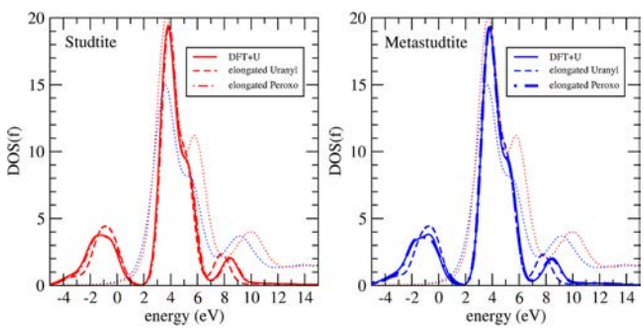

Figure 6. *f* DOS calculated with the DFT+*U* method for relaxed DFT +*U* structures (solid lines) with elongated U−O uranyl (dashed lines) and peroxo (dotted−dashed lines, which overlap solid lines and are indistinguishable) bond lengths. The dotted lines represent the experimentally determined U M edge HR XANES.

DOS values of studtite and metastudtite with elongated U−O_{peroxo} bonds remain unchanged, while elongating the U═O_{axial} distance (Figure 6) or bending the U═O_{axial} bond (Figure 5) shifts the position of the 5f σ^* transition toward lower energies (higher binding energies), consistent with the method used to fit the HR XANES spectra. From these results, the bending of the uranyl moiety is not conclusively ruled out.

In addition to the changes in the uranium based DOS, there are also differences in the oxygen DOS (Figure 7). The largest differences are in the DOS associated with the peroxo group (∼1 eV shift to a higher energy in metastudtite), while the U═O_{axial} oxygens also shift but by ∼0.1 eV, consistent with the changes in bond lengths from both experiment and theory.

CONCLUSION

In this work, we have presented X ray based spectroscopic characterization of studtite and metastudtite. XPS showed that there were differences in the U $4f_{7/2}$ peak for studtite, the highest reported binding energy, compared to that of metastudtite, and there were also differences in the O 1s region, though this peak was too broad to assign definitively to specific bondings. X ray spectroscopy at the uranium M_4 edge

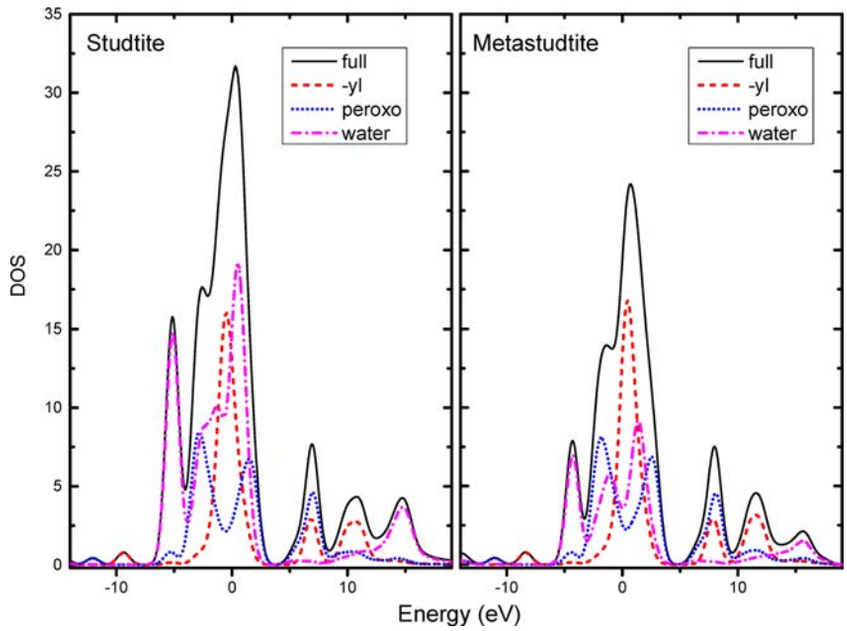

Figure 7. Oxygen DOS calculated with the DFT+*U* method for relaxed structures.

indicates that the overlap driven covalence of the U═O_{axial} bond decreases upon dehydration. Finally, time resolved luminescence spectroscopy at near liquid helium temperature shows a well resolved spectrum for studtite with a dominant lifetime of 862 μs; in contrast, metastudtite shows a broad, poorly resolved spectrum with a much reduced lifetime of 28 μs. A theoretical investigation, benchmarked to the X ray spectroscopy data, has also been undertaken, and the 3d to 5f σ^* transition appears to be the most sensitive to variations in the U═O_{axial} bond length. Although not conclusive, some experimental and theoretical evidence suggests that a bending of the uranyl fragment could occur during dehydration. Taken together, we have shown that the dehydration of studtite does have significant structural and electronic perturbations of the uranyl moiety.

EXPERIMENTAL SECTION

Studtite, metastudtite,[50] and metaschoepite[24] were prepared as described in the literature. XPS measurements were performed with a PHI 5000 VersaProbe II (ULVAC PHI Inc.) instrument equipped with a scanning microprobe X ray source [monochromatic Al Kα (1486.7 eV) X rays]. Charge compensation at isolating samples was obtained by combination of an electron flood gun and a floating ion gun generating low energy electrons (1.1 eV) and low energy argon ions (8 eV) (dual beam technique), respectively. Survey scans were recorded with a pass energy of 187.85 eV of the analyzer. Narrow scans of the elemental lines were recorded at a 23.5 eV pass energy and yield an energy resolution of 0.69 eV fwhm at the Ag $3d_{5/2}$ elemental line of pure silver. Calibration of the binding energy scale of the spectrometer was performed using well established binding energies of elemental lines of pure metals (monochromatic Al Kα, Cu $2p_{3/2}$ at 932.62 eV and Au $4f_{7/2}$ at 83.96 eV).[25] The error in the binding energies of elemental lines is estimated to ±0.2 eV at isolating samples. Powder samples were pressed onto an indium foil and mounted on the sample holder. All spectra were charge referenced to C 1s (hydrocarbon) at 285.0 eV. Data analysis was performed using ULVAC PHI MultiPak, version 9.6.

The instrumentation and experimental procedures for luminescence spectroscopic measurement at near liquid helium temperature have been described previously.[38,51] Briefly, crystalline grains of the minerals were placed in 2 mm × 4 mm × 30 mm fused quartz cuvettes, and the cuvettes were capped with silicone stoppers and then attached to the coldfinger of a CryoIndustries RC152 cryostat with liquid helium vaporizing beneath the sample to reach a temperature of 8 ± 2 K. Time resolved luminescence emission spectra of the samples were recorded via excitation at 415 nm with a Spectra Physics Nd:YAG laser pumped Lasertechnik GWU MOPO laser. The emitted light was collected at 85° to the excitation beam, dispersed through an Acton SpectroPro 300i double monochromator spectrograph, and detected with a thermoelectrically cooled Princeton Instruments PIMAX intensified CCD camera that was triggered by the delayed output of the laser pulse and controlled by the WinSpec data acquisition software. The photoluminescence decay curves were constructed by plotting the spectral intensity of a series of time delayed luminescence spectra as a function of the corresponding delay time. The emission spectra and decay data were analyzed using commercial software, IGOR, from Wavematrix, Inc.

The HR XANES measurements were performed at the INE Beamline, ANKA synchrotron radiation facility, Karlsruhe, Germany. Note that the HR XANES is also termed partial fluorescence yield XANES (PFY XANES) and high energy resolution fluorescence detected XANES (HERFD XANES), and these abbreviations are used for the same experimental technique. Twenty milligrams from each uranyl compound was ground with cellulose powder (100 mg) and pressed into 1 cm diameter pellets that were of homogeneous character. The pellets were covered with two Kapton films with 8 and 13 μm thicknesses. The primary X ray beam was vertically collimated by a cylindrically bent Rh coated mirror, monochromatized by a Si(111) double crystal monochromator, and focused by a toroidal double focusing Rh coated mirror to 500 μm × 500 μm onto the sample. For a detailed description of the INE Beamline, see ref 52. The multianalyzer crystals Johann type spectrometer (MAC spectrometer) was used. The sample, crystals, and detector were positioned on a Rowland circle in the vertical plane with a diameter of 1 m equal to the bending radius of the spherically bent analyzer crystals. The emitted U M_β fluorescence line was diffracted by five Si(220) analyzer crystals (Saint Gobain Crystals) set at a 75.17° Bragg angle and focused onto a VITUS silicon drift detector (VITUS SDD KETEK). The experimental energy resolution was estimated to 1.2 eV by measuring the fwhm of the elastically scattered peak. For the U M_4 edge (3728 eV) HR XANES measurements, the MAC spectrometer was set at the maximum of the U M_β emission line (75.17° Bragg angle), whereas the primary energy was scanned to obtain U M_4 edge HR XANES spectra. The energy positions of the features of the U M_4

edge HR XANES spectra (A–D) were determined by modeling the spectra with Fityk[53] (Figure S3), and the values are listed in Table S2.

X ray powder diffraction patterns were recorded on a Siemens D500 instrument using a Bragg–Brentano geometry with a step size of 0.02° at 16 s for metstudtite. Rietveld refinements were performed using the GSAS with EXPGUI.[54] The structure of metastudtite predicted by Weck et al.[46] was used as a starting model for the refinement.

Computational Studies. The *ab initio* calculations of studtite and metastudtite were performed using the plane wave DFT package Quantum Espresso.[55] A PBE exchange correlation functional[56] and ultrasoft pseudopotentials were used to mimic the presence of core electrons.[57] The plane wave energy cutoff was set to 50 Ry, and all the calculations were spin polarized assuming an antiferromagnetic spin arrangement. The DFT+*U* methodology was used to better capture the strongly correlated character of f states. The value of the Hubbard *U* parameter was derived *ab initio* using the approach of Cococcioni and de Gironcoli;[58] we obtained a value of 2.6 eV for both phases. We have extensively tested this method on a wide range of uranium bearing molecules and solids and obtained good results for the structure and thermochemistry of these materials.[59] In our models, the studtite and metastudtite unit cells contained 68 and 44 atoms, respectively. We used the 2 × 3 × 3 and 2 × 2 × 3 Methfessel Paxton k point grids[60] for calculations of studtite and metastudtite, respectively, which were chosen to give the convergence of the considered energies within 0.1 kJ/mol. In the DFT+*U* calculations, we utilized the maximally localized Wannier functions as projectors. This approach led to a much better representation of f orbitals than when atomic orbitals were used, which was reflected by more realistic, nearly zero occupations of f orbitals.

AUTHOR INFORMATION

Corresponding Authors

*Telephone: +353 1 8963501. E mail: bakerrj@tcd.ie.

*Telephone: +49 721 608 24024. E mail: tonya.vitova@kit.edu.

*Telephone: +49 2461 61 9356. E mail: p.kowalski@fz juelich.de.

ORCID

Tonya Vitova: 0000 0002 3117 7701

Robert J. Baker: 0000 0003 1416 8659

Present Address

#S.B.: Department of Chemistry, Katwa College, Katwa, West Bengal 713130, India.

Author Contributions

R.J.B., T.V., and P.M.K. devised the project. I.P. and T.V. conducted and analyzed the XAS measurements, D.S. the XPS measurements, and Z.W. the cryogenic photoluminescence measurements. S.B. synthesized the materials. The *ab initio* calculations and relevant discussion were performed by G.B. and P.M.K., and the Rietvelt refinement was analyzed by P.W.D. The manuscript was written through contributions of all authors. All authors have given approval to the final version of the manuscript.

Notes

The authors declare no competing financial interest.

ACKNOWLEDGMENTS

R.J.B. and T.V. thank TALISMAN (TAL C03 02) for funding. S.B. thanks the Irish Research Council for a postdoctoral fellowship. T.V. acknowledges the Helmholtz Association of German Research Centres for Grant VH NG 734. G.B. and P.M.K. acknowledge the JARA HPC initiative for time on the RWTH Aachen and Forschungszentrum Jülich GmbH supercomputing resources awarded through JARA HPC Partition. The authors acknowledge Synchrotron Light Source ANKA for provision of instruments at their beamlines. Part of this work was conducted at the William R. Wiley Environmental Molecular Sciences Laboratory (EMSL), a national scientific user facility located at the Pacific Northwest National Laboratory (PNNL) and sponsored by the U.S. Department of Energy's Office of Biological and Environmental Research (BER).

REFERENCES

(1) (a) Kim, K. W.; Hyun, J. T.; Lee, K. Y.; Lee, E. H.; Lee, K. W.; Song, K. C.; Moon, J. K. Effects of the different conditions of uranyl and hydrogen peroxide solutions on the behavior of the uranium peroxide precipitation. *J. Hazard. Mater.* **2011**, *193*, 52–58. (b) Clarens, F.; de Pablo, J.; Casas, I.; Giménez, J.; Rovira, M.; Merino, J.; Cera, E.; Bruno, J.; Quiñones, J.; Martínez Esparza, A. The oxidative dissolution of unirradiated UO_2 by hydrogen peroxide as a function of pH. *J. Nucl. Mater.* **2005**, *345*, 225–231. (c) Clarens, F.; de Pablo, J.; Díez Pérez, I.; Casas, I.; Giménez, J.; Rovira, M. *Environ. Sci. Technol.* **2004**, *38*, 6656–6661. (d) Amme, M.; Renker, B.; Schmid, B.; Feth, M. P.; Bertagnolli, H.; Döbelin, W. Raman microspectrometric identification of corrosion products formed on UO_2 nuclear fuel during leaching experiments. *J. Nucl. Mater.* **2002**, *306*, 202–212. (e) Diaz Arocas, P.; Quiñones, J.; Maffiotte, C.; Serrano, J.; Garcia, J.; Almazan, J. R.; Esteban, J. Esteban, Effect of Secondary Phases Formation in the Leaching of UO_2 Under Simulated Radiolytic Products. *MRS Online Proc. Libr.* **1994**, *353*, 641–648.

(2) Sattonnay, G.; Ardois, C.; Corbel, C.; Lucchini, J. F.; Barthe, M. F.; Garrido, F.; Gosset, D. Alpha radiolysis effects on UO_2 alteration in water. *J. Nucl. Mater.* **2001**, *288*, 11–19.

(3) Clarens, F.; Giménez, J.; de Pablo, J.; Casas, I.; Rovira, M.; Dies, J.; Quiñones, J.; Martínez Esparza, A. Influence of β radiation on UO_2 dissolution at different pH values. *Radiochim. Acta* **2005**, *93*, 533–538.

(4) Jegou, C.; Muzeau, B.; Broudic, V.; Peuget, S.; Poulesquen, A.; Roudil, D.; Corbel, C. Effect of external gamma irradiation on dissolution of the spent UO_2 fuel matrix. *J. Nucl. Mater.* **2005**, *341*, 62–82.

(5) Abrefah, J.; Marschmann, S.; Jenson, E. D. Examination of the Surface Coatings Removed from K East Basin Fuel Elements. Technical Report PNNL 11806; Pacific Northwest National Laboratory: Richland, WA, 1998.

(6) Wang, Y.; von Gunten, K.; Bartova, B.; Meisser, N.; Astner, M.; Burger, M.; Bernier Latmani, R. Products of in Situ Corrosion of Depleted Uranium Ammunition in Bosnia and Herzegovina Soils. *Environ. Sci. Technol.* **2016**, *50*, 12266–12274.

(7) Wilbraham, R. J.; Boxall, C.; Goddard, D. T.; Taylor, R. J.; Woodbury, S. E. The effect of hydrogen peroxide on uranium oxide films on 316L stainless steel. *J. Nucl. Mater.* **2015**, *464*, 86–96.

(8) Goff, G. S.; Brodnax, L. F.; Cisneros, M. R.; Peper, S. M.; Field, S. E.; Scott, B. L.; Runde, W. H. First Identification and Thermodynamic Characterization of the Ternary U(VI) Species, $UO_2(O_2)(CO_3)_2^{4-}$, in UO_2–H_2O_2–K_2CO_3 Solutions. *Inorg. Chem.* **2008**, *47*, 1984–1990.

(9) Meca, S.; Martinez Torrents, A.; Marti, V.; Gimenez, J.; Casas, I.; de Pablo, J. Determination of the equilibrium formation constants of two U(VI)–peroxide complexes at alkaline pH. *Dalton Trans.* **2011**, *40*, 7976–7982.

(10) (a) Zanonato, P. L.; Di Bernardo, P.; Grenthe, I. Chemical equilibria in the binary and ternary uranyl(VI)–hydroxide–peroxide systems. *Dalton Trans.* **2012**, *41*, 3380–3386. (b) Martínez Torrents,

A.; Meca, S.; Baumann, N.; Martí, V.; Giménez, J.; de Pablo, J.; Casas, I. Uranium speciation studies at alkaline pH and in the presence of hydrogen peroxide using time resolved laser induced fluorescence spectroscopy. *Polyhedron* **2013**, *55*, 92−101.

(11) Nyman, M.; Rodriguez, M. A.; Campana, C. F. Self Assembly of Alkali Uranyl Peroxide Clusters. *Inorg. Chem.* **2010**, *49*, 7748−7755.

(12) For recent reviews, see: (a) Burns, P. C. Nanoscale uranium based cage clusters inspired by uranium mineralogy. *Mineral. Mag.* **2011**, *75*, 1−25. (b) Qiu, J.; Burns, P. C. Clusters of Actinides with Oxide, Peroxide, or Hydroxide Bridges. *Chem. Rev.* **2013**, *113*, 1097−1120. (c) Nyman, M.; Burns, P. C. A comprehensive comparison of transition metal and actinyl polyoxometalates. *Chem. Soc. Rev.* **2012**, *41*, 7354−7367.

(13) Armstrong, C. R.; Nyman, M.; Shvareva, T.; Sigmon, G. E.; Burns, P. C.; Navrotsky, A. Uranyl peroxide enhanced nuclear fuel corrosion in seawater. *Proc. Natl. Acad. Sci. U. S. A.* **2012**, *109*, 1874−1877.

(14) (a) Blanchard, F.; Ellart, M.; Rivenet, M.; Vigier, N.; Hablot, I.; Morel, B.; Grandjean, S.; Abraham, F. Role of Ammonium Ions in the Formation of Ammonium Uranyl Peroxides and Uranyl Peroxo oxalates. *Cryst. Growth Des.* **2016**, *16*, 200−209. (b) Ling, J.; Wallace, C. M.; Szymanowski, J. E. S.; Burns, P. C. Hybrid uranium oxalate fullerene topology cage clusters. *Angew. Chem., Int. Ed.* **2010**, *49*, 7271−7273. (c) Ling, J.; Qiu, J.; Burns, P. C. Uranyl Peroxide Oxalate Cage and Core−Shell Clusters Containing 50 and 120 Uranyl Ions. *Inorg. Chem.* **2012**, *51*, 2403−2408.

(15) Dembowski, M.; Olds, T. A.; Pellegrini, K. L.; Hoffmann, C.; Wang, X.; Hickam, S.; He, J.; Oliver, A. G.; Burns, P. C. Solution (31) P NMR Study of the Acid Catalyzed Formation of a Highly Charged $\{U_{24}Pp_{12}\}$ Nanocluster, $[(UO_2)_{24}(O_2)_{24}(P_2O_7)_{12}]^{48}$, and Its Structural Characterization in the Solid State Using Single Crystal Neutron Diffraction. *J. Am. Chem. Soc.* **2016**, *138*, 8547−8553.

(16) Hughes Kubatko, K. A.; Helean, K. B.; Navrotsky, A.; Burns, P. C. Stability of Peroxide Containing Uranyl Minerals. *Science* **2003**, *302*, 1191−1193.

(17) Guo, X.; Ushakov, S. V.; Labs, S.; Curtius, H.; Bosbach, D.; Navrotsky, A. Energetics of metastudtite and implications for nuclear waste alteration. *Proc. Natl. Acad. Sci. U. S. A.* **2014**, *111*, 17737−17742.

(18) Rey, A.; Casas, I.; Giménez, J.; Quiñones, J.; de Pablo, J. Effect of temperature on studtite stability: Thermogravimetry and differential scanning calorimetry investigations. *J. Nucl. Mater.* **2009**, *385*, 467−473.

(19) Odoh, S. A.; Shamblin, J.; Colla, C. A.; Hickam, S.; Lobeck, H. L.; Lopez, R. A. K.; Olds, T.; Szymanowski, J. E. S.; Sigmon, G. E.; Neuefeind, J.; Casey, W. H.; Lang, M.; Gagliardi, L.; Burns, P. C. Structure and Reactivity of X ray Amorphous Uranyl Peroxide, U_2O_7. *Inorg. Chem.* **2016**, *55*, 3541−3546.

(20) Guo, X.; Wu, D.; Xu, H.; Burns, P. C.; Navrotsky, A. Thermodynamic studies of studtite thermal decomposition pathways via amorphous intermediates UO_3, U_2O_7, and UO_4. *J. Nucl. Mater.* **2016**, *478*, 158−163.

(21) Thomas, R.; Rivenet, M.; Berrier, E.; deWaele, I.; Arab, M.; Amaraggi, D.; Morel, B.; Abraham, F. Thermal decomposition of $(UO_2)O_2(H_2O)_2{\cdot}2H_2O$: Influence on structure, microstructure and hydrofluorination. *J. Nucl. Mater.* **2017**, *483*, 149−157.

(22) Burns, P. C.; Hughes, K. A. Studtite, $[(UO_2)\ (O_2)\ (H_2O)_2]\ (H_2O)_2$: The first structure of a peroxide mineral. *Am. Mineral.* **2003**, *88*, 1165−1168.

(23) Walshe, A.; Prüßmann, T.; Vitova, T.; Baker, R. J. An EXAFS and HR XANES study of the uranyl peroxides $[UO_2(\eta^2\ O_2)(H_2O)_2]{\cdot}nH_2O$ (n = 0, 2) and uranyl (oxy)hydroxide $[(UO_2)_4O(OH)_6]{\cdot}6H_2O$. *Dalton. Trans.* **2014**, *43*, 4400−4407.

(24) Altmaier, M.; Yalçintaş, E.; Gaona, X.; Neck, V.; Müller, R.; Schlieker, M.; Fanghänel, T. Solubility of U(VI) in chloride solutions. I. The stable oxides/hydroxides in NaCl systems, solubility products, hydrolysis constants and SIT coefficients. *J. Chem. Thermodyn.* **2017**, *114*, 2−13.

(25) Seah, M. P.; Gilmore, I. S.; Beamson, G. XPS: binding energy calibration of electron spectrometers 5—re evaluation of the reference energies. *Surf. Interface Anal.* **1998**, *26*, 642−649.

(26) Schindler, M.; Hawthorne, F. C.; Freund, M. S.; Burns, P. C. XPS spectra of uranyl minerals and synthetic uranyl compounds. I: The U 4f spectrum. *Geochim. Cosmochim. Acta* **2009**, *73*, 2471−2487.

(27) Using the metaschoepite structure as initial lattice parameters and atomic configurations: Weller, M. T.; Light, M. E.; Gelbrich, T. Structure of uranium (VI) oxide dihydrate $UO_3{\cdot}2H_2O$; synthetic meta schoepite $(UO_2)_4O(OH)_6{\cdot}5H_2O$. *Acta Crystallogr., Sect. B: Struct. Sci.* **2000**, *56*, 577−583.

(28) See for example: Cole, R. J.; Macdonald, B. F.; Weightman, P. Relative core level shifts in XPS: a theoretical study. *J. Electron Spectrosc. Relat. Phenom.* **2002**, *125*, 147−152.

(29) (a) Johansson, L. I.; Hagström, A. L.; Jacobson, B. E.; Hagström, S. B. M. ESCA studies of core level shifts and valence band structure in nonstoichiometric single crystals of titanium carbide. *J. Electron Spectrosc. Relat. Phenom.* **1977**, *10*, 259−271. (b) Taucher, T. C.; Hehn, I.; Hofmann, O. T.; Zharnikov, M.; Zojer, E. Understanding Chemical versus Electrostatic Shifts in X ray Photoelectron Spectra of Organic Self Assembled Monolayers. *J. Phys. Chem. C* **2016**, *120*, 3428−3437.

(30) Schindler, M.; Hawthorne, F. C.; Freund, M. S.; Burns, P. C. XPS spectra of uranyl minerals and synthetic uranyl compounds. II: The O 1s spectrum. *Geochim. Cosmochim. Acta* **2009**, *73*, 2488−2509.

(31) Vitova, T.; Kvashnina, K. O.; Nocton, G.; Sukharina, G.; Denecke, M. A.; Butorin, S. M.; Mazzanti, M.; Caciuffo, R.; Soldatov, A.; Behrends, T.; Geckeis, H. High energy resolution x ray absorption spectroscopy study of uranium in varying valence states. *Phys. Rev. B: Condens. Matter Mater. Phys.* **2010**, *82*, 235118.

(32) (a) Vitova, T.; Denecke, M. A.; Göttlicher, J.; Jorissen, K.; Kas, J. J.; Kvashnina, K.; Prüßmann, T.; Rehr, J. J.; Rothe, J. Actinide and lanthanide speciation with high energy resolution X ray techniques. *J. Phys.: Conf. Ser.* **2013**, *430*, 012117. (b) Kvashnina, K. O.; Butorin, S. M.; Martin, P.; Glatzel, P. Chemical State of Complex Uranium Oxides. *Phys. Rev. Lett.* **2013**, *111*, 253002. (c) Vitova, T.; Pidchenko, I.; Fellhauer, D.; Bagus, P. S.; Joly, Y.; Pruessmann, T.; Bahl, S.; Gonzalez Robles, E.; Rothe, J.; Altmaier, M.; Denecke, M. A.; Geckeis, H. The role of the 5f valence orbitals of early actinides in chemical bonding. *Nat. Commun.* **2017**, *8*, 16053. (d) Pidchenko, I.; Kvashnina, K. O.; Yokosawa, T.; Finck, N.; Bahl, S.; Schild, D.; Polly, R.; Bohnert, E.; Rossberg, A.; Gottlicher, J.; Dardenne, K.; Rothe, J.; Schafer, T.; Geckeis, H.; Vitova, T. Uranium Redox Transformations after U(VI) Coprecipitation with Magnetite Nanoparticles. *Environ. Sci. Technol.* **2017**, *51*, 2217−2225.

(33) Vitova, T.; Green, J. C.; Denning, R. G.; Loble, M.; Kvashnina, K.; Kas, J. J.; Jorissen, K.; Rehr, J. J.; Malcherek, T.; Denecke, M. A. Polarization Dependent High Energy Resolution X ray Absorption Study of Dicesium Uranyl Tetrachloride. *Inorg. Chem.* **2015**, *54*, 174−182.

(34) Written by Visscher, L.; Jensen, H. J.; Saue, T. Contributions from Bast, R.; Dubillard, S.; Dyall, K. G.; Ekström, U.; Eliav, E.; Fleig, T.; Gomes, A. S. P.; Helgaker, T. U.; Henriksson, J.; Iliaš, M.; Jacob, Ch. R.; Knecht, S.; Norman, P.; Olsen, J.; Pernpointner, M.; Ruud, K.; Sałek, P.; Sikkema, J. *DIRAC, a relativistic ab initio electronic structure program*, release DIRAC08; 2008 (http://dirac.chem.sdu.dk).

(35) Bunau, O.; Joly, Y. Self consistent aspects of x ray absorption calculations. *J. Phys.: Condens. Matter* **2009**, *21*, 345501.

(36) Podkovyrina, Y.; Pidchenko, I.; Prüßmann, T.; Bahl, S.; Göttlicher, J.; Soldatov, A.; Vitova, T. Probing Covalency in the UO_3 Polymorphs by U M_4 edge HR XANES. *J. Phys.: Conf. Ser.* **2016**, *712*, 012092.

(37) Mallon, C.; Walshe, A.; Forster, R. J.; Keyes, T. E.; Baker, R. J. Physical Characterization and Reactivity of the Uranyl Peroxide $[UO_2(\eta^2\ O_2)(H_2O)_2]{\cdot}2H_2O$: Implications for Storage of Spent Nuclear Fuels. *Inorg. Chem.* **2012**, *51*, 8509−8515.

(38) (a) Wang, Z.; Zachara, J. M.; Yantasee, W.; Gassman, P. L.; Liu, C.; Joly, A. G. Cryogenic Laser Induced Fluorescence Characterization of U(VI) in Hanford Vadose Zone Pore Waters. *Environ. Sci. Technol.*

2004, *38*, 5591−5597. (b) Wang, Z.; Zachara, J. M.; Liu, C.; Gassman, P. L.; Felmy, A. R.; Clark, S. B. A cryogenic fluorescence spectroscopic study of uranyl carbonate, phosphate and oxyhydroxide minerals. *Radiochim. Acta* **2008**, *96*, 591−598.

(39) Bastians, S.; Crump, G.; Griffith, W. P.; Withnall, R. Raspite and studtite: Raman spectra of two unique minerals. *J. Raman Spectrosc.* **2004**, *35*, 726−731.

(40) Mishra, R. K.; Sudarsan, V.; Jain, S.; Kaushik, C. P.; Vatsa, R. K.; Tyagi, A. K. Structural and Luminescence Studies on Barium Sodium Borosilicate Glasses Containing Uranium Oxides. *J. Am. Ceram. Soc.* **2014**, *97*, 427−431.

(41) (a) Schöne, S.; Radoske, T.; März, J.; Stumpf, T.; Patzschke, M.; Ikeda Ohno, A. $[UO_2Cl_2(phen)_2]$, a Simple Uranium(VI) Compound with a Significantly Bent Uranyl Unit (phen = 1,10 phhenanthrolin). *Chem. Eur. J.* **2017**, *23*, 13574−13578. (b) Pedrick, E. A.; Schultz, J. W.; Wu, G.; Mirica, L. M.; Hayton, T. W. Perturbation of the O U O Angle in Uranyl by Coordination to a 12 Membered Macrocycle. *Inorg. Chem.* **2016**, *55*, 5693−5701. (c) Silver, M. A.; Dorfner, W. L.; Cary, S. K.; Cross, J. N.; Lin, J.; Schelter, E. J.; Albrecht Schmitt, T. E. Why Is Uranyl Formohydroxamate Red? *Inorg. Chem.* **2015**, *54*, 5280−5284. (d) Kiernicki, J. J.; Cladis, D. P.; Fanwick, P. E.; Zeller, M.; Bart, S. C. Synthesis, Characterization, and Stoichiometric U−O Bond Scission in Uranyl Species Supported by Pyridine(diimine) Ligand Radicals. *J. Am. Chem. Soc.* **2015**, *137*, 11115−11125. (e) Lu, E.; Cooper, O. J.; McMaster, J.; Tuna, F.; McInnes, E. J. L.; Lewis, W.; Blake, A. J.; Liddle, S. T. Synthesis, Characterization, and Reactivity of a Uranium(VI) Carbene Imido Oxo Complex. *Angew. Chem., Int. Ed.* **2014**, *53*, 6696−6700. (f) Tourneux, J. C.; Berthet, J. C.; Cantat, T.; Thuery, P.; Mezailles, N.; Ephritikhine, M. Exploring the Uranyl Organometallic Chemistry: From Single to Double Uranium−Carbon Bonds. *J. Am. Chem. Soc.* **2011**, *133*, 6162−6165. (g) Berthet, J. C.; Thuery, P.; Dognon, J. P.; Guillaneux, D.; Ephritikhine, M. Sterically Congested Uranyl Complexes with Seven Coordination of the UO_2 Unit: the Peculiar Ligation Mode of Nitrate in $[UO_2(NO_3)_2(Rbtp)]$ Complexes. *Inorg. Chem.* **2008**, *47*, 6850−6862. (h) Maynadie, J.; Berthet, J. C.; Thuery, P.; Ephritikhine, M. The first cyclopentadienyl complex of uranyl. *Chem. Commun.* **2007**, 486−488. (i) Wilkerson, M. P.; Burns, C. J.; Morris, D. E.; Paine, R. T.; Scott, B. L. Steric Control of Substituted Phenoxide Ligands on Product Structures of Uranyl Aryloxide Complexes. *Inorg. Chem.* **2002**, *41*, 3110−3120. (j) Dyall, K. G. Bonding and bending in the actinyls. *Mol. Phys.* **1999**, *96*, 511−518.

(42) Hayton, T. W. Understanding the origins of O_{yl} U O_{yl} bending in the uranyl unit. *Dalton Trans.* **2018**, *47*, 1003.

(43) Deliens, M.; Piret, P. Metastudtite, $UO_4{\cdot}2H_2O$, a new mineral from Shinkolobwe, Shaba, Zaire. *Am. Mineral.* **1983**, *68*, 456−458.

(44) Rodriguez, M. A.; Weck, P. E.; Sugar, J. D.; Kulp, T. J. Powder X ray diffraction of Metastudtite, $(UO_2)O_2(H_2O)_2$. *Powder Diffr.* **2016**, *31*, 71−72.

(45) Ostanin, S.; Zeller, P. Ab initio study of uranyl peroxides: Electronic factors behind the phase stability. *Phys. Rev. B: Condens. Matter Mater. Phys.* **2007**, *75*, 073101.

(46) Weck, P. F.; Kim, E.; Jové Colón, C. F.; Sassani, D. C. Structures of uranyl peroxide hydrates: a first principles study of studtite and metastudtite. *Dalton Trans.* **2012**, *41*, 9748−9752.

(47) Blanca Romero, A.; Kowalski, P. M.; Beridze, G.; Schlenz, H.; Bosbach, D. Performance of DFT+U method for prediction of structural and thermodynamic parameters of monazite type ceramics. *J. Comput. Chem.* **2014**, *35*, 1339−1346.

(48) Perdew, J. P.; Ruzsinszky, A.; Csonka, G. I.; Vydrov, O. A.; Scuseria, G. E.; Constantin, L. A.; Zhou, X.; Burke, K. Restoring the Density Gradient Expansion for Exchange in Solids and Surfaces. *Phys. Rev. Lett.* **2008**, *100*, 136406.

(49) Colmenero, F.; Bonales, L. J.; Cobos, J.; Timon, V. Study of the thermal stability of studtite by in situ Raman spectroscopy and DFT calculations. *Spectrochim. Acta, Part A* **2017**, *174*, 245−253.

(50) Debets, P. C. X ray diffraction data on hydrated uranium peroxide. *J. Inorg. Nucl. Chem.* **1963**, *25*, 727−730.

(51) Wang, Z.; Zachara, J. M.; Gassman, P. L.; Liu, C.; Qafoku, O.; Yantasee, W.; Catalano, J. G. Fluorescence spectroscopy of U(VI) silicates and U(VI) contaminated Hanford sediment. *Geochim. Cosmochim. Acta* **2005**, *69*, 1391−1403.

(52) Rothe, J.; Butorin, S.; Dardenne, K.; Denecke, M. A.; Kienzler, B.; Löble, M.; Metz, V.; Seibert, A.; Steppert, M.; Vitova, T.; Walther, C.; Geckeis, H. The INE Beamline for actinide science at ANKA. *Rev. Sci. Instrum.* **2012**, *83*, 043105.

(53) Wojdyr, M. Fityk: a general purpose peak fitting program. *J. Appl. Crystallogr.* **2010**, *43*, 1126−1128.

(54) Larson, A. C.; Von Dreele, R. B. General Structure Analysis System (GSAS). Technical Report LAUR 86 748; Los Alamos National Laboratory: Los Alamos, NM, 1994. Toby, B. H. EXPGUI, a graphical user interface for GSAS. *J. Appl. Crystallogr.* **2001**, *34*, 210−213.

(55) Giannozzi, P.; Baroni, S.; Bonini, N.; Calandra, M.; Car, R.; Cavazzoni, C.; Ceresoli, D.; Chiarotti, G. L.; Cococcioni, M.; Dabo, I.; Dal Corso, A.; de Gironcoli, S.; Fabris, S.; Fratesi, G.; Gebauer, R.; Gerstmann, U.; Gougoussis, C.; Kokalj, A.; Lazzeri, M.; Martin Samos, L.; Marzari, N.; Mauri, F.; Mazzarello, R.; Paolini, S.; Pasquarello, A.; Paulatto, L.; Sbraccia, C.; Scandolo, S.; Sclauzero, G.; Seitsonen, A. P.; Smogunov, A.; Umari, P.; Wentzcovitch, R. M. QUANTUM ESPRESSO: a modular and open source software project for quantum simulations of materials. *J. Phys.: Condens. Matter* **2009**, *21*, 395502.

(56) Perdew, J. P.; Burke, K.; Ernzerhof, M. Generalized Gradient Approximation Made Simple. *Phys. Rev. Lett.* **1996**, *77*, 3865−3868.

(57) Vanderbilt, D. Soft self consistent pseudopotentials in a generalized eigenvalue formalism. *Phys. Rev. B: Condens. Matter Mater. Phys.* **1990**, *41*, 7892−7895.

(58) Cococcioni, M.; de Gironcoli, S. Linear response approach to the calculation of the effective interaction parameters in the LDA + U method. *Phys. Rev. B: Condens. Matter Mater. Phys.* **2005**, *71*, 035105.

(59) Beridze, G.; Kowalski, P. M. Benchmarking the DFT+U Method for Thermochemical Calculations of Uranium Molecular Compounds and Solids. *J. Phys. Chem. A* **2014**, *118*, 11797−11810.

(60) Methfessel, M.; Paxton, A. T. High precision sampling for Brillouin zone integration in metals. *Phys. Rev. B: Condens. Matter Mater. Phys.* **1989**, *40*, 3616−3621.